Hindawi
Geofluids
Volume 2021, Article ID 6165366, 13 pages
https://doi.org/10.1155/2021/6165366

Research Article

A Study of Acoustic Emission and Damage Evolution of Limestone under Different Stress Paths and Confining Pressures

Jianjun Zhao,[1] **Xun Wan**,[1] **Lan Ji**,[1] **Jinshi Zhu**,[2] **Xinran Dai**,[1] **and Jun Wang**[1]

[1]*State Key Laboratory of Geohazard Prevention and Geoenvironment Protection (Chengdu University of Technology), 610059 Chengdu, China*
[2]*Three Gorges Geotechnical Consultants Co., Ltd., 430074 Wuhan, China*

Correspondence should be addressed to Jianjun Zhao; j.j.zhao@qq.com

Received 19 August 2021; Accepted 18 September 2021; Published 19 October 2021

Academic Editor: Haojie Lian

Buried depth is an important factor affecting the deformation and failure of gob surrounding rock. Basing on triaxial compression unloading test and acoustic emission (AE) of limestone under three different initial confining pressures (5 MPa, 10 MPa, and 20 MPa) and three different stress paths, we analyzed the deformation and failure characteristics and energy releasing process of the virgin rock, the gob overburden rock, and the gob sidewall rock with different buried depths (within 1000 m). The results showed that, with the increase of buried depth, the shear fracture mainly propagated and the failure mode of the gob sidewall rock changed from brittleness to plasticity; however, the gob overburden rock was all brittle failure. Compared with shallow buried depths, the energy releasing triggered by confining pressure reduction in deep buried depths was more concentrated and intense. Under the background of deep buried depths, the peak strength and residual strength of the gob sidewall rock were the lowest, and the damage variable was the largest. We proposed that the first "acute phase" of AE can be wielded as the precursor information of the gob sidewall rock failure and crack propagation of hydraulic fracturing. The findings of the study are beneficial for the disaster prevention and control of deep mining in mountainous area, as well as fracturing evaluation.

1. Introduction

With the consumption and utilization of coal resources, deep mining gradually tends to be normalized, and the coal mines with mining depth close to 1000 m are increasing yearly [1, 2]. Under the influence of deep in situ stress and mining disturbance, the gob surrounding rock shows nonlinear mechanical characteristics [3], which further lead to large-scale geohazards. In mountainous areas of Guizhou, China, the stress redistribution of gob surrounding rock after mining further induces deformation of overburden rock and coal pillar failure and even the whole instability of slope [4–6]. We investigated the mining forms and slope structure conditions of some mines in mountainous areas of Guizhou (Table 1), which have the following common characteristics: (a) large buried depth span of coal seam (160~1100 m); (b) small dip angle of coal seam (8~12°); (c) medium-thick coal seam (1.59~3.6 m); (d) limestone, sandstone, siltstone, and other hard rocks exist in the roof; and (e) longwall mining method adopted. Among them, the buried depth of coal seam determines the initial in situ stress conditions of gob surrounding rock, affecting the deformation of gob overburden rock and gob sidewall rock [7]. However, the deformation and failure characteristics and instability prediction of gob surrounding rock affected by buried depth were rarely studied by scholars.

In shallow underground mining, the failure of gob surrounding rock limited in a small area usually occurs after a period of accelerated deformation. However, in deep mining, the destruction of gob surrounding rock is often large scale [8]. It is an important prerequisite to understand the deformation and failure characteristics of gob sidewall rock and overburden rock under the influence of mining-induced stress redistribution. Many scholars have studied the laboratory mechanical tests of different rocks under various stress paths [9–11]. Furthermore, the use of AE brings more precursory

Table 1: Mining forms and slope structure conditions of some mines in mountainous areas of Guizhou.

	Faer mine	Lvtang mine	Yongsheng mine	Qingshan mine	Zuojiaying mine	Daqing mine	Guobao mine
Location	Liupanshui city	Bijie city	Bijie city	Duyun city	Bijie city	Bijie city	Xingren county
Depth of coal seams (m)	300~1020	220~1000	200~1000	160~900	280~1100	400~1050	600~1000
Coal seam plunge (°)	10	10	8	10	12	12	8
Average thickness of coal seams (m)	2.8	1.99	2.65	3.6	1.7	2.35	1.59
Direct roof lithology	Mudstone	Siltstone	Limestone	Sandstone	Limestone	Pelitic siltstone	Limestone, marlstone
Indirect roof lithology	Pelitic siltstone	Packsand, limestone	Limestone	Macker	Limestone	Limestone	Limestone
Coal mining method	Longwall mining method						

information of rock deformation and failure and can even be used as a reliable method to identify fracture propagation during hydraulic fracturing [12, 13]. The process energy releasing law based on AE characteristic parameters has been studied a lot [14], and a series of damage constitutive relations have been proposed [15]. Under specific geological background, the deformation and failure characteristics of rock under different stress paths and confining pressures have been proved to be able to reflect the deformation properties of gob surrounding rock [16]. Hence, it is necessary to study the deformation and failure characteristics of gob surrounding rock based on the stress-strain relations and energy releasing law.

The background of this study is the growing deep mining operations in mountainous areas of Guizhou Province. Basing on triaxial compression unloading experiment and AE test, we studied the deformation and failure characteristics of gob sidewall rock and overburden rock under different buried depths. The findings of the study would be useful for strength characteristics and failure predicting of gob surrounding rock under different buried depths and also provide some inspiration for the evaluation of deep hydraulic fracturing.

2. Experimental Material, System, and Procedures

2.1. Test Specimens and Apparatus. In this study, as the overburden and sidewall rock of the gob, the thick limestone of Feixianguan Formation of the Lower Triassic, which is exposed from the mining slope of Daqing Coal Mine in Nayong County, Guizhou Province, was selected as the experimental object. According to the rock test standards of the International Society for Rock Mechanics (ISRM) [17], cylindrical samples with a diameter of 50 mm and a length of 100 mm were prepared. In order to avoid the discretization of experimental results, all samples are prepared from the same rock mass, the cutting direction is perpendicular to the rock layer, and the samples do not contain the layers and primary joints [18].

The MTS815 Flex Test GT triaxial rock mechanics test system was used for the test (Figure 1), which can provide normal load capacity up to 4600 kN and maximum allowable

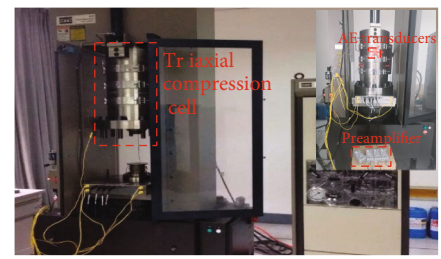

Figure 1: MTS815 Flex Test GT triaxial rock mechanics test system and Micro-II Digital AE System.

confining pressure 140 MPa. Linear variable differential transformer (LVDT) was used to obtain the full stress-strain curve of the rock. The Micro-II Digital AE System was used to monitor the acoustic signal of material fracture. Before the test, four AE sensors were symmetrically fixed on the pressure chamber (Figure 1), and the adhesive was Vaseline. In the test, the threshold of acoustic emission amplitude was set at 40 dB to eliminate the influence of environmental noise. The elastic wave generated by rock fracture is received by the sensors after passing through the cold shrinkable tube on the sample surface, hydraulic oil, and the outer wall of the pressure chamber, which will weaken the intensity of the AE signal, which is inevitable. However, this measurement method has little influence on the determination of characteristic AE signals such as yield, macroscopic fracture, and friction sliding between fracture surfaces [16].

2.2. Testing Scheme. Deep mining is often met with huge gob surrounding rock stress. We collected the original stress data at different buried depths and calculated the equivalent confining pressure at different buried depths. According to the statistical results in Table 2, in the range of buried depth less than 1000 m, excluding data noise, the confining pressure fluctuates within 5~20 MPa [19–21]. In this study, the confining pressures of 5 MPa, 10 MPa, and 20 MPa were selected to simulate the original rock stress under different buried depths.

Under the same confining pressure (that is, the same buried depth), three different stress paths were considered to represent the stress environment of the virgin rock

Table 2: Statistic results of original rock stress in some underground engineering in China (with the downdip angle as positive) [19–21].

Number	Project	Buried depth	Maximum principal stress			Intermediate principal stress			Minimum principal stress			Equivalent confining pressure
			Value (MPa)	Azimuth (°)	Plunge (°)	Value (MPa)	Azimuth (°)	Plunge (°)	Value (MPa)	Azimuth (°)	Plunge (°)	Value (MPa)
1	Hebi Six Mine	447.66	32.50	258.07	12.35	22.16	101.54	75.56	4.07	349.21	5.19	5.47
2	Jiaozuo Jiulishan Mine	318.70	8.85	357.59	74.80	5.70	192.08	14.53	1.06	101.12	8.9	5.60
3	Lianshao Niumasi Mine	556.57	21.78	87.99	18.56	17.43	282.23	70.89	1.86	170.46	4.38	5.31
4	Beipiao Guanshan Mine	989.05	52.96	34.79	11.25	30.85	148.24	63.45	13.23	299.77	23.71	6.57
5	Xinwen Suncun Mine	870	38.13	100.1	24.2	28.35	79.2	61.5	1.61	14.8	14.1	14.27
6	Jinping II Hydropower Station Tunnel	169	10.9	157	-3	7.2	70	50	6.5	64	-40	9.59
7		169	12.5	139	-18	11.1	39	-29	7.9	77	55	13.57
8		259	16.79	106	-11.04	10.9	23	-27.6	8.9	35.5	59.9	14.05
9		317	11.11	126	-24	7.7	1	-52	5.17	50	27	8.51
10		616	19.11	148	58	9.97	326	31	7.19	56	1	11.17
11		1079	40.69	146	49	18.81	75	-16	12.82	177	-36	18.88

(Scheme 1), gob overburden rock (Scheme 2), and gob sidewall rock (Scheme 3) (Figure 2). In a short time after the formation of the gob, the gob overburden hard strata still bear the gravity of the strata below the ground surface. Furthermore, the lateral constraints of the gob boundary gradually disappear, leading to the development of tensile fractures extending upward from the gob boundary, resulting in a small confining pressure reduction of the gob overburden rock [22]. Without the support of the coal seam, the gravity of the rock above the extracted panel will be completely borne by the gob sidewall rock, leading to the rapid concentration of axial stress on the sidewall rock. The decrease of confining pressure makes the sidewall rock exposed to adverse stress environment.

Different stress path schemes were designed as follows (Figure 3). In order to ensure the representativeness of results, each experimental condition was repeated for 3 times, and AE counting was carried out throughout the whole process.

For each experimental scheme, the confining pressure was first increased to the preset value (5 MPa, 10 MPa, and 20 MPa) at a constant rate of 0.5 MPa/s. Considering that the change of confining pressure of overburden rock lags behind the sidewall rock, the unloading rate of confining pressure of Scheme 2 was set in this paper to be less than that of Scheme 3.

Scheme 1. Axial load is applied to sample at a constant rate of 0.1 MPa/s until the specimen fails.

Scheme 2. Increase the axial load at a rate of 0.1 MPa/s to 0.8 q_u (q_u is the peak compressive strength of the rock in Scheme 1). With the axial load unchanged, the confining pressure is reduced at a rate of 0.1 MPa/s until the specimen fails.

Scheme 3. Increase the axial load at a rate of 0.1 MPa/s to 0.6 q_u, and then, decrease the confining pressure at a constant rate of 0.2 MPa/s and continue to increase the axial load at a constant rate of 0.1 MPa/s until the specimen fails.

In each experiment scheme, the confining pressure was kept unchanged, and the residual strength was obtained by continuous axial compression.

3. Results

In this part, the stress and strain characteristics and process energy releasing of rock deformation and failure under different experimental settings are analyzed. In the process of compression deformation of rock specimens, the initiation, expansion, and coalescence of microcracks often result in energy releasing, and the magnitude of which can be directly characterized by AE counting. The damage variable defined by AE counting is used to characterize the whole process of energy releasing. Considering that the rock still retains different degrees of residual strength after failure under different loading conditions [14], the damage variable D' is defined as

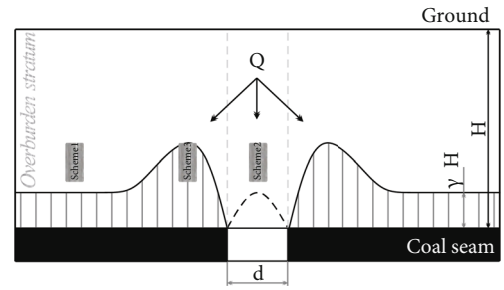

Figure 2: The stress environment of gob surrounding rock (d: the width of open-off cut; γ: unit weight of rock; H: thickness of rock; Q: weight of gob overburden rock).

$$D' = \left(1 - \frac{\sigma_c}{\sigma_d}\right) \times \frac{C_d}{C_0}, \tag{1}$$

where σ_c is the residual strength, σ_d is the peak compressive strength, C_d is the cumulative ringing count at any time, and C_0 is the cumulative ringing count in the whole process.

According to the ringing count and the characteristics of damage variables, the deformation and failure of rock under different test conditions can be divided into three periods, namely, A—the quiet phase, B—the transition phase, and C—the acute phase.

3.1. The Virgin Rock. The confining pressure was kept constant throughout the test process for studying the mechanical properties of the virgin rock at different buried depths. Figures 4 and 5 show the whole process of stress-strain relations under three different confining pressures and the fracture sketch after failure. It is obvious that with the increase of confining pressure, the peak compressive strength increases significantly, and the elastic modulus increases slightly. We determined the primary and secondary fractures by observing the sequence and the width of fractures, the fracture sketch shows that the failure mode of rock changes from brittleness to ductility, and the increase of confining pressure leads to more secondary fractures in the failure process, which intersect with the main fractures to form several groups of "shear joints." See in Figure 6, under the confining pressure of 5 MPa, the rock deformation and failure experience "A-C-A," which is manifested as the energy short-term releasing, and brittle failure occurs after the completion of the releasing of high-level energy. Under 10 MPa, the rock deformation and failure experience "B-C-A," and part of the energy releasing occurs in the elastic deformation stage. The "acute phase" starts almost at the same time as the plastic deformation, and the residual strength appears after the end of the "acute phase," and then, it enters the "quiet phase." Under 20 MPa, the rock deformation and failure experience "A-B-C-A." Compared with the condition of low confining pressure, the energy releasing is less in elastic deformation stage, and the "acute phase" starts only after the partial plastic deformation of the rock. It can be seen that the increase of confining pressure brings the hysteresis of energy releasing.

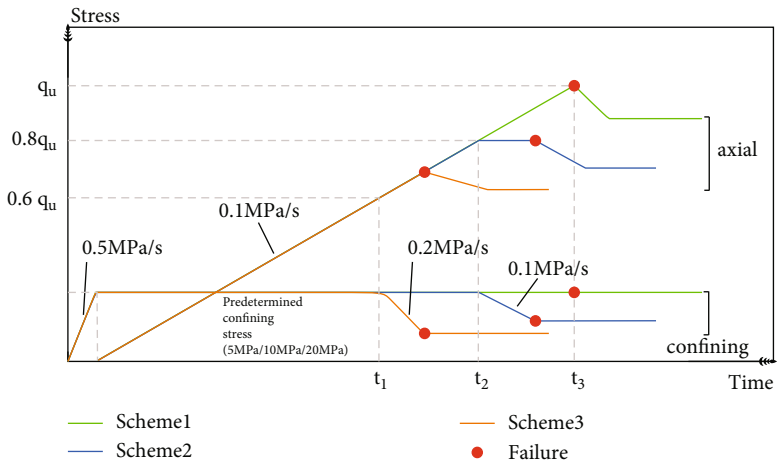

Figure 3: The experimental design of three stress paths (q_u is the peak compressive strength under different confining pressures in Scheme 1; t_1 and t_2 represent the moment when the confining pressure in Schemes 3 and 2 begins to change, and t_3 represents the moment when the sample in Scheme 1 is in peak stress).

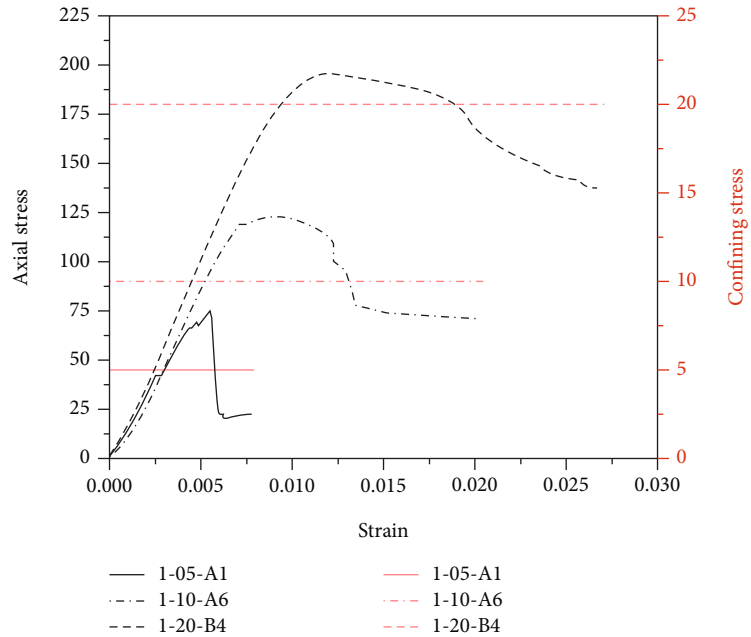

Figure 4: Axial stress/confining pressure-strain relations of Scheme 1 under different confining pressures.

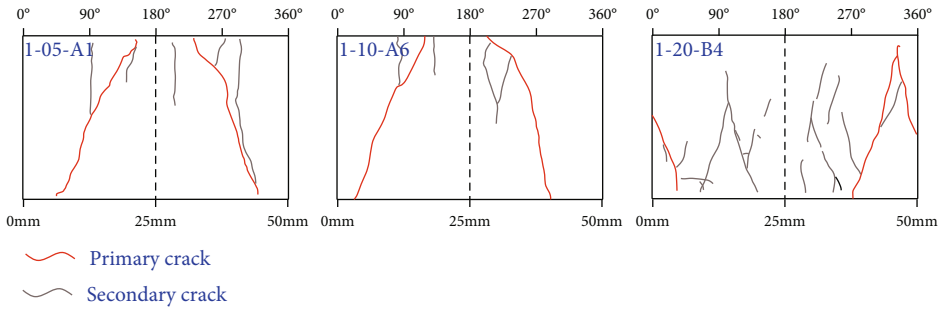

Figure 5: Sketch of fractures after failure of Scheme 1 under different confining pressures.

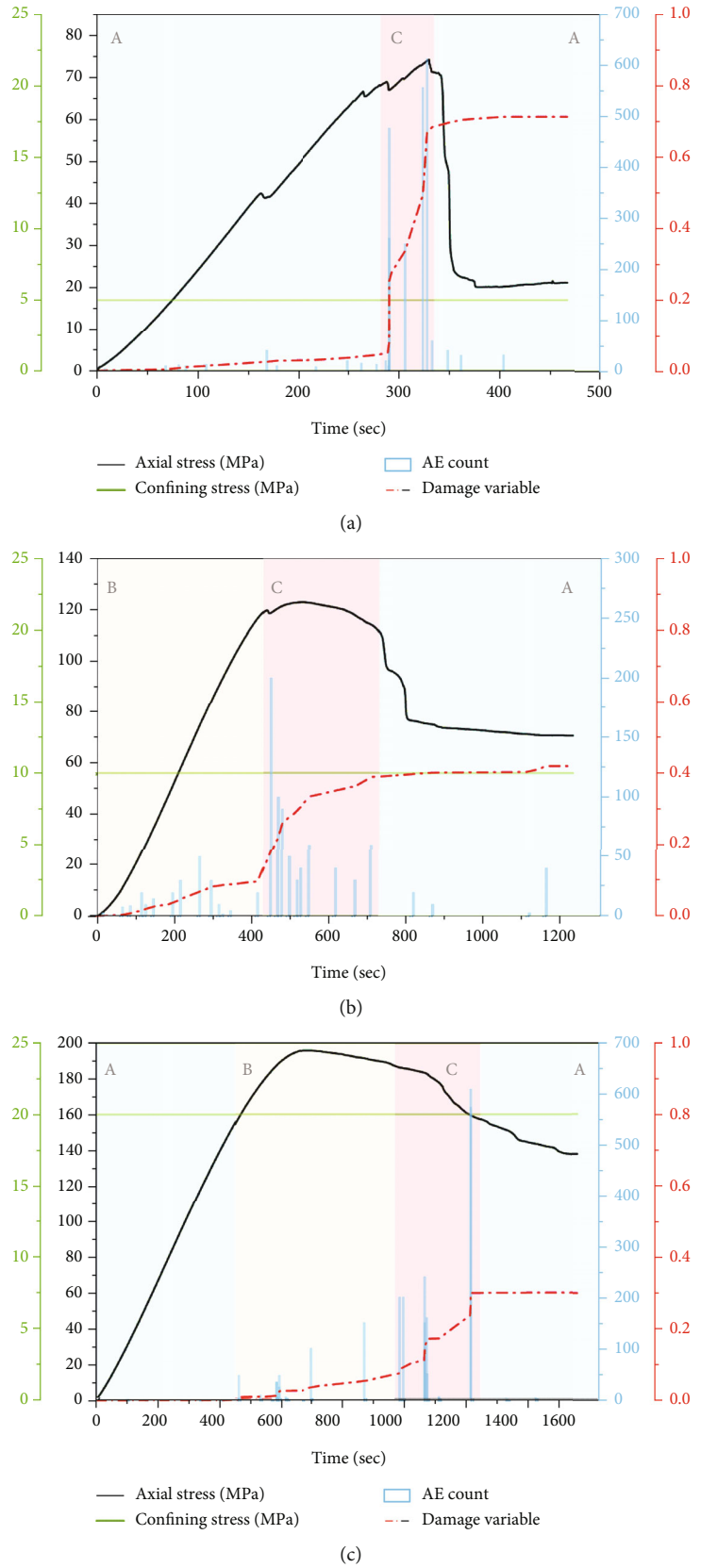

Figure 6: AE ringing count/damage variable-time relations of Scheme 1 under different confining pressures (confining pressure setting: (a) 5 MPa, (b) 10 MPa, and (c) 20 MPa).

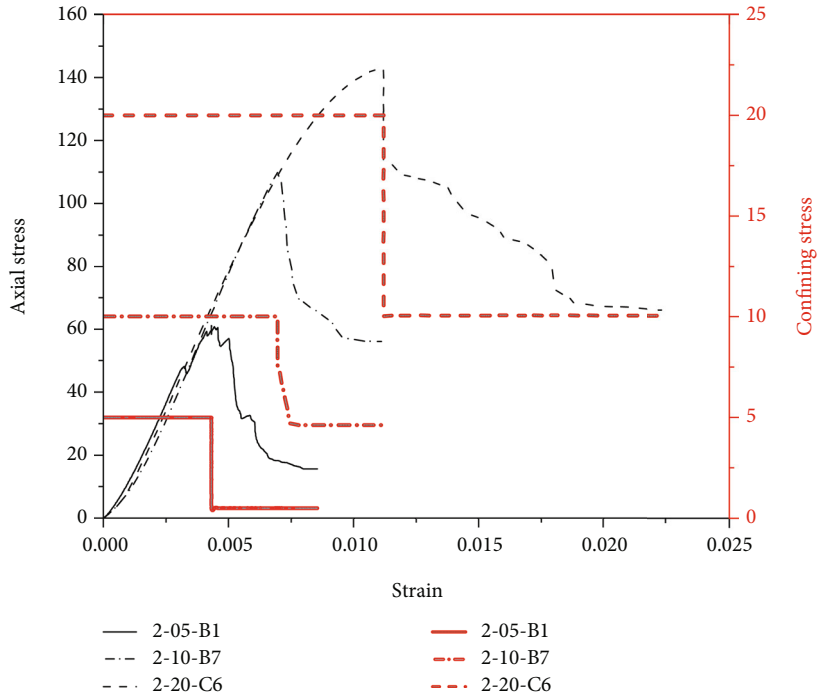

Figure 7: Axial stress/confining pressure-strain relations of Scheme 2 under different confining pressures.

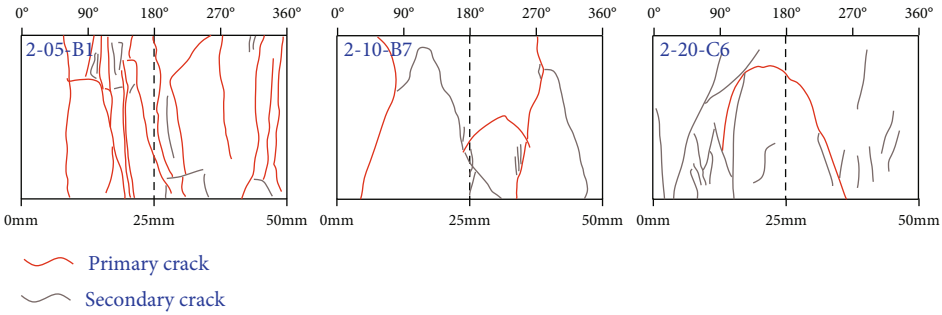

Figure 8: Sketch of fractures after failure of Scheme 2 under different confining pressures.

3.2. The Gob Overburden Rock. Under different confining pressure conditions, the rock presents brittle failure, and the axial stress drop almost appears when the confining pressure decreases (Figure 7). Under 20 MPa, the postpeak residual deformation is larger. Under low confining pressure, the deformation and failure are controlled by tensile crack, while under high confining pressure they are controlled by shear crack (Figure 8). See in Figure 9, under 5 MPa, the rock deformation and failure experience "A-C-A." Obviously, confining pressure unloading causes a longer "acute phase," in which "the acute phase" mainly contains two major energy releasing events, the first one occurs before the unloading stage of confining pressure and the second one in the postpeak stress adjustment stage. The energy releasing at the second one may be caused by further dislocations of the coarse joints inside the rock [16]. Under 10 MPa, the rock deformation and failure experience "A-B-C-A," and the unloading of confining pressure, plastic deformation, and the beginning of the "acute phase" appear almost at the same time. Under 20 MPa, the rock deformation and failure experience "A-B-C-A," which is different from the energy releasing of the virgin rock. The plastic deformation starts almost at the same time as the "acute phase," and sustain time is slightly longer.

3.3. The Gob Sidewall Rock. With the increase of confining pressure, the failure form changes from brittleness failure to plasticity failure. However, different from the virgin rock, the threshold value of confining pressure required by the transition from brittleness to plasticity becomes higher in this case (Figure 10). The deformation and failure are controlled by the "tension-shear" composite crack, and the failure tends to

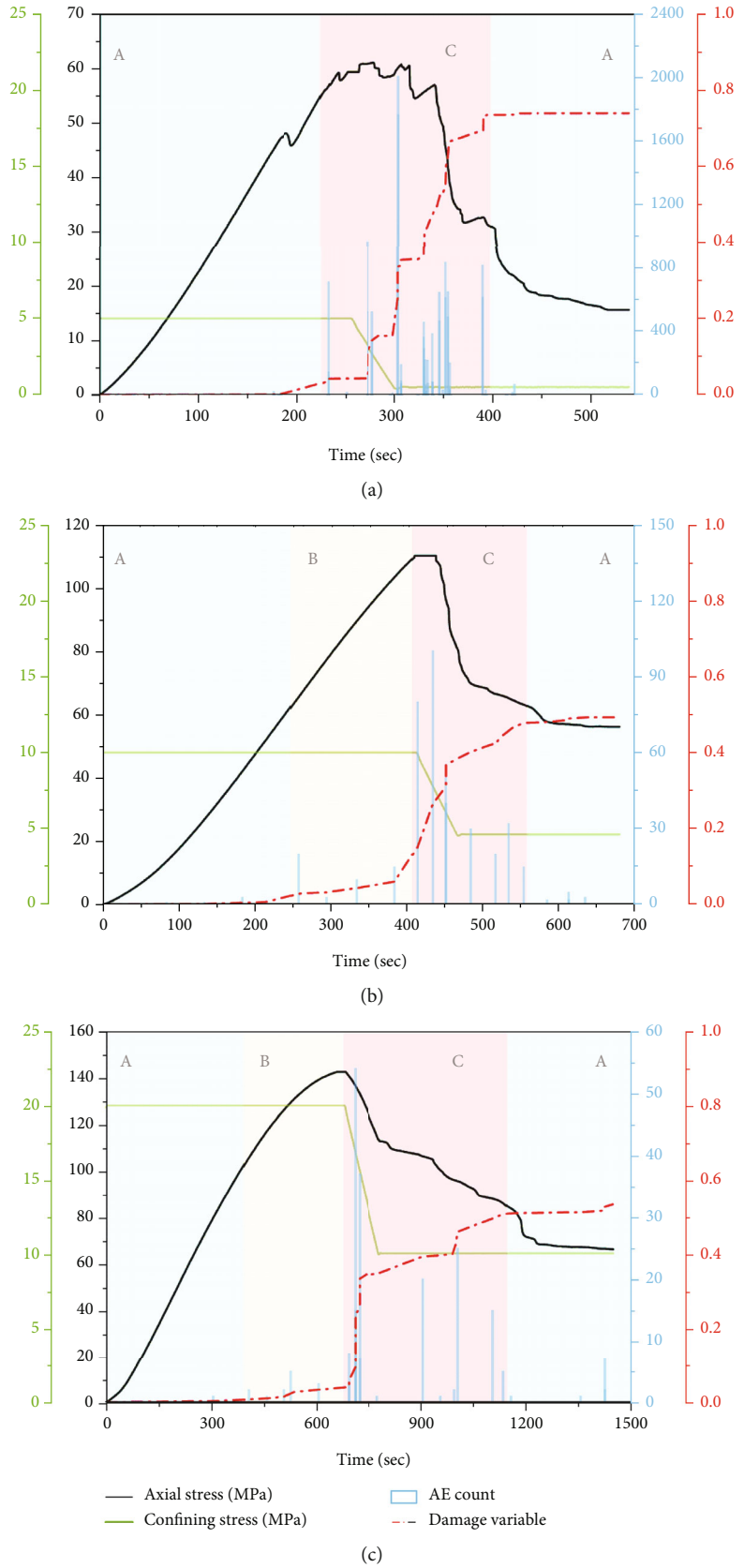

Figure 9: AE ringing count/damage variable-time relations of Scheme 2 under different confining pressures (confining pressure setting: (a) 5 MPa, (b) 10 MPa, and (c) 20 MPa).

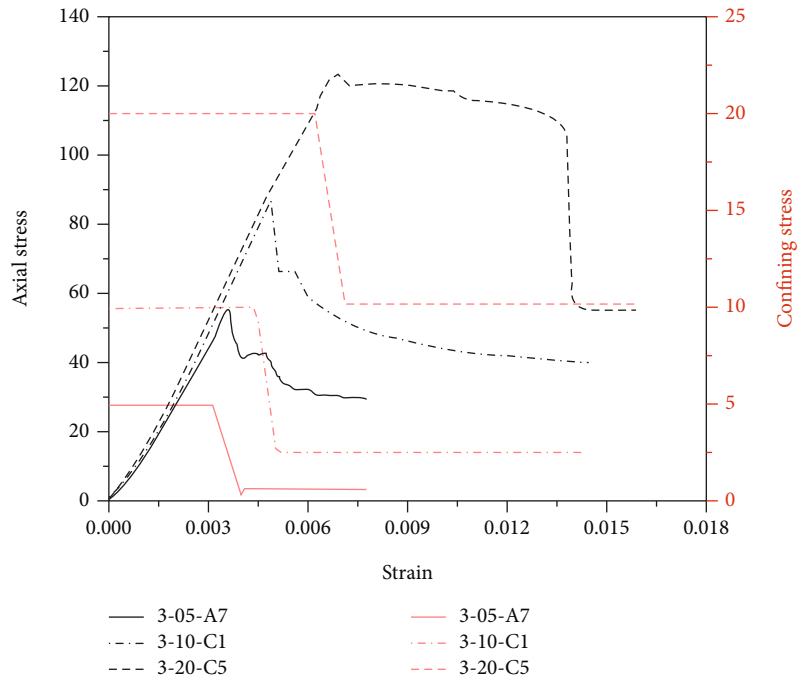

Figure 10: Axial stress/confining pressure-strain relations of Scheme 3 under different confining pressures.

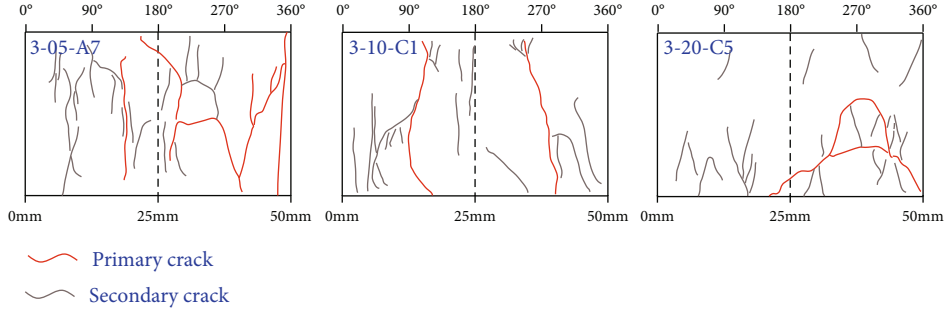

Figure 11: Sketch of fractures after failure of Scheme 3 under different confining pressures.

integrate from fragmentation with the increase of confining pressure (Figure 11). See in Figure 12, under 5 MPa, the rock deformation and failure experienced "A-C-A," and the unloading of confining pressure triggered the energy releasing in the "acute phase." The first postpeak stress drop event did not release too much energy, and after the stress adjustment in the later period, there appeared an energy release event with the largest ring count. Under 10 MPa, the rock deformation and failure experience "A-C-B-A." Similarly, the unloading of confining pressure almost happens at the same time as the energy releasing in the "acute phase." A large amount of energy is released near the peak compressive strength, and a small amount of energy is released in the residual deformation stage. Under 20 MPa, rock deformation and failure experience "A-C-B-C-A," the unloading of confining pressure causes the energy releasing of the first "acute phase," and as the rock strain softening phenomenon, a small number of AE signal is received. After the accumulation of deformation, the second "acute phase" occurs, the axial stress drops rapidly, and then, the residual deformation occurs. Obviously, under low confining pressure, the advance reduction of confining pressure makes the energy releasing in the "acute phase" more dispersed and the duration longer. With the increase of the initial confining pressure (buried depth), the failure mode of the rock changes from brittleness to plasticity and causes several "acute phases."

4. Discussion

Table 3 statistics the peak compressive strength, residual strength, and damage variables of the virgin rock, the gob overburden rock, and the gob sidewall rock under different confining pressures (buried depths).

For peak compressive strength and residual strength: compared with the virgin rock and the gob overburden rock, the gob sidewall rock always has the lowest peak compressive

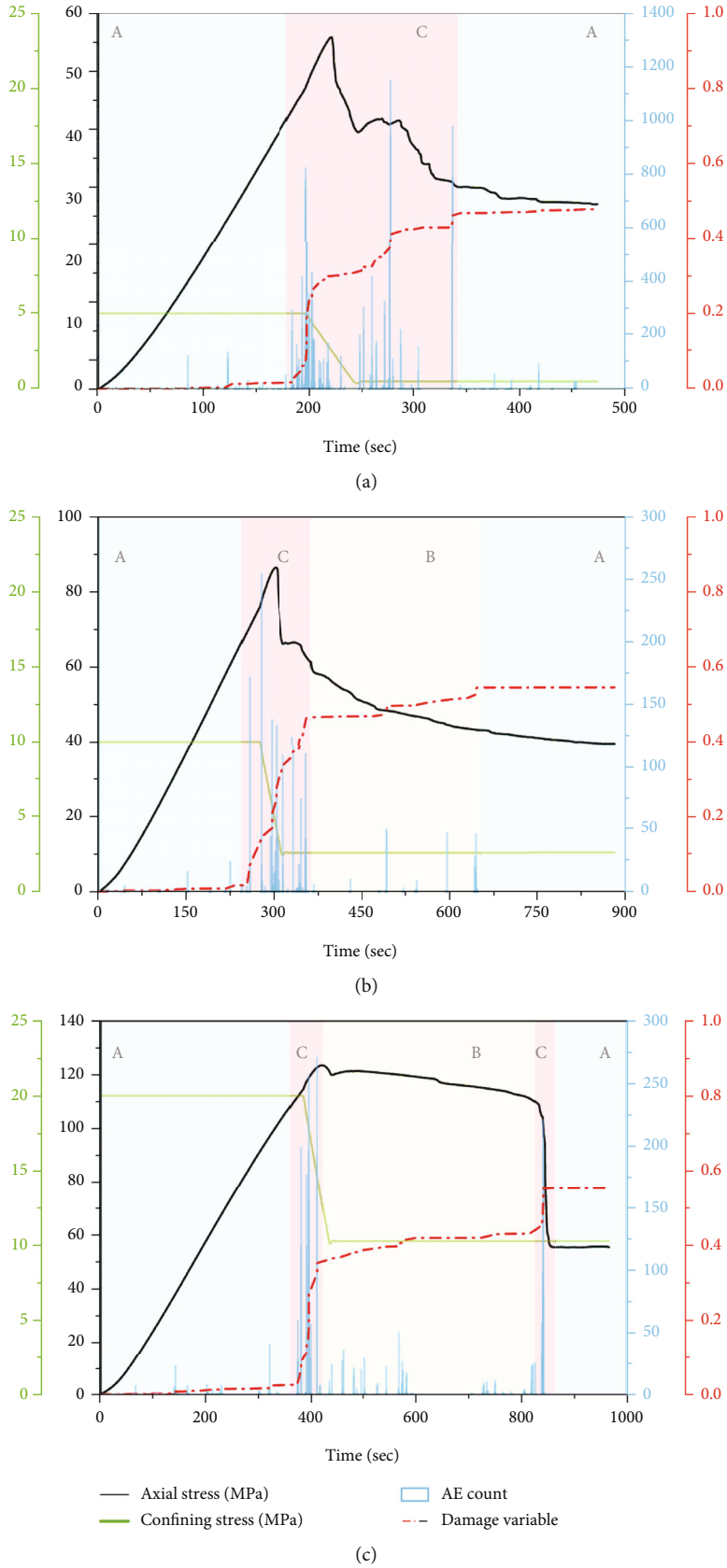

Figure 12: AE ringing count/damage variable-time relations of Scheme 3 under different confining pressures (confining pressure setting: (a) 5 MPa, (b) 10 MPa, and (c) 20 MPa).

Table 3: The mechanics and damage characteristic values of each scheme.

	Specimen number	Confining stress (MPa)	Peak strength (MPa)	Residual strength (MPa)	Damage variable
Scheme 1	A1	5	74.63	21.11	0.712
	A6	10	123.29	70.55	0.419
	B4	20	196.38	137.66	0.298
Scheme 2	B1	5	60.10	15.64	0.740
	B7	10	110.46	56.08	0.492
	C6	20	143.01	66.63	0.534
Scheme 3	A7	5	56.54	29.55	0.477
	C1	10	87.59	39.46	0.545
	C5	20	123.92	55.24	0.552

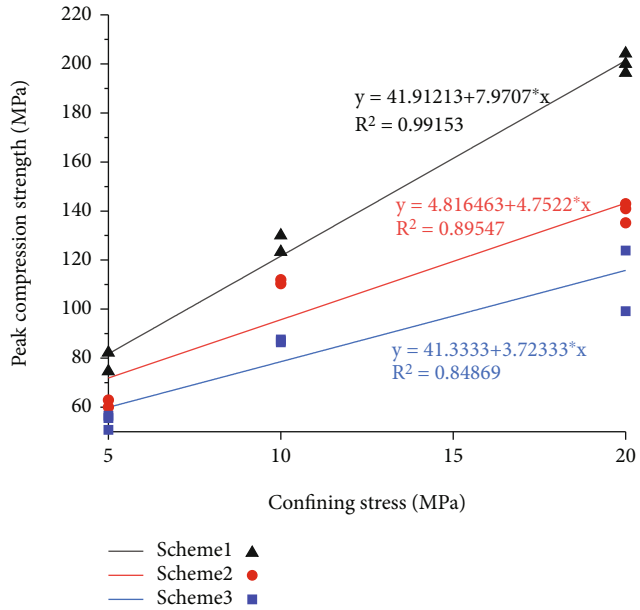

Figure 13: The peak compressive strength of each scheme.

strength under different confining pressures (Figure 13). After the stress redistribution, the probability of instability failure is great. Cai et al. [23] and Liang et al. [16] proposed that the gob surrounding rock with higher residual strength tends to have a smaller yield range, and the residual strength is of great significance to underground construction and support design. By comparing the experimental results in this paper, it is found that the increase of confining pressure can effectively improve the residual strength of the gob overburden rock and sidewall rock. In addition, the residual strength of the gob overburden rock is the minimum when the confining pressure is 5 MPa, while the residual strength of the gob sidewall rock is the minimum when the confining pressure is 10 MPa or 20 MPa.

For damage variables: with the increase of confining pressure, the damage variables of the virgin rock, the gob overburden rock, and the gob sidewall rock show the characteristics of gradually decreasing, decreasing first and then increasing, and gradually increasing, respectively. Under 5 MPa, the damage variable of the gob overburden rock is the largest (value is up to 0.740). Under 10 MPa and 20 MPa, the damage variable of the gob sidewall rock is the largest (value is 0.545 and 0.552, respectively).

According to the above analysis of peak compressive strength, residual strength, and damage variables, it is shown that with the increase of confining pressure (buried depth), the gob sidewall rock is the most vulnerable to damage and the degree of damage is the largest. Therefore, the gob sidewall rock is the key point of disaster prevention during deep mining in mountainous area. Furthermore, horizontal wells are more stable than vertical ones during deep hydraulic fracturing. As can be seen from Figure 12, with the increase of confining pressure, the failure mode of the gob sidewall rock changes from brittleness to plasticity. Under high confining pressure (20 MPa), rock failure occurs after two "acute phases." Therefore, the "acute phase" of AE for the first time can be used as the precursor information of the failure of the gob sidewall rock under high confining pressure. The precursor information of surrounding rock failure under high

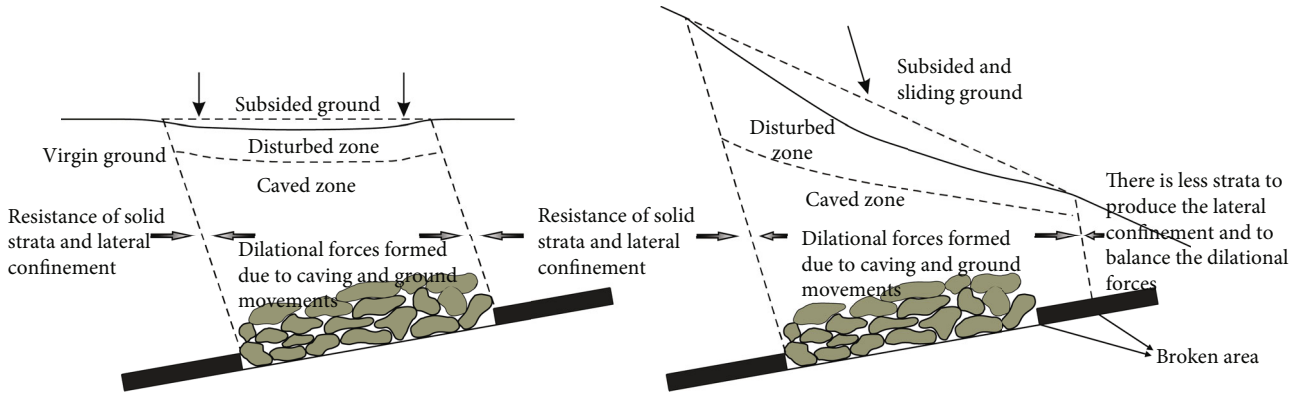

Figure 14: The gob overburden rock stress state of flat/sloping terrain in mountainous areas ((a) flat terrain and (b) sloping terrain, adapted from [6]).

pressure determined by the "acute phase" of AE can also be used to predict the formation of fracture network during hydraulic fracturing.

It should be noted that, under the background of mining in mountainous areas, the change of stress environment of the gob overlying rock is extremely complex in a long time after mining (Figure 14). In order to quantify the deformation and failure properties of the gob surrounding rock more accurately, the authors will consider the influence of complex stress paths on the gob overburden rock in the further study.

5. Conclusion

Three different initial confining pressures were set, and triaxial compression unloading tests were carried out on limestone under different stress paths. The deformation and failure characteristics of the virgin rock, the gob overburden rock, and the gob sidewall rock under different confining pressures (buried depths) were studied. Meanwhile, the damage variables were obtained through the whole-process AE monitoring. Based on the analysis of the experimental results, the failure precursors of the gob sidewall rock in deep mining (within 1000 m) are proposed.

The main conclusions are as follows:

(1) The gob sidewall rock has higher confining pressure threshold of brittle-plastic transformation than the virgin rock, while the gob overburden rock has brittle failure at different confining pressures (buried depths).

(2) Under 10 MPa and 20 MPa, the unloading of confining pressure triggers the immediate energy releasing of the gob overburden rock and sidewall rock. However, under 5 MPa, the unloading of the confining pressure causes the energy releasing of the gob overburden rock and sidewall rock to be more dispersed, and part of the energy can only be released in the postpeak stress adjustment stage. In addition, the increase of confining pressure (buried depths) will cause a lag in the energy releasing of the virgin rock.

(3) With the increase of confining pressure (buried depth), the part with the greatest damage degree changes from the gob overburden rock to the sidewall rock, and the peak compressive strength and residual strength of the sidewall rock are the lowest under the background of deep mining.

(4) Under the background of deep mining in mountainous areas, the gob sidewall rock mainly appears plastic failure, and the "acute phase" of AE for the first time can be used as the precursor information for the failure of the gob sidewall rock and crack propagation of hydraulic fracturing.

Data Availability

The AE and triaxial compression unloading data used to support the findings of this study are available from the corresponding author upon request.

Conflicts of Interest

The authors declare that they have no conflicts of interest.

Acknowledgments

The research present in this manuscript is funded by the Science and Technology Plan Project of Sichuan Province (Grant No. 2021YJ0053), National Natural Science Foundation of China (Grant No. 41877273), Innovative Research Groups of the National Natural Science Foundation of China (Grant No. 41521002), and State Key Laboratory of Geohazard Disaster Prevention and Geoenvironment Protection (Chengdu University of Technology) (Grant No. SKLGP2017Z016). These supports are gratefully acknowledged.

References

[1] L. Driad-Lebeau, F. Lahaie, M. Al Heib, J. P. Josien, P. Bigarré, and J. F. Noirel, "Seismic and geotechnical investigations following a rockburst in a complex French mining district,"

International Journal of Coal Geology, vol. 64, no. 1-2, pp. 66–78, 2005.

[2] A. G. Yardimci and M. Karakus, "A new protective destressing technique in underground hard coal mining," *International Journal of Rock Mechanics and Mining Sciences*, vol. 130, article 104327, 2020.

[3] Z. L. Li, X. Q. He, L. M. Dou, D. Z. Song, and G. F. Wang, "Numerical investigation of load shedding and rockburst reduction effects of top-coal caving mining in thick coal seams," *International Journal of Rock Mechanics and Mining Sciences*, vol. 110, pp. 266–278, 2018.

[4] E. Fathi Salmi, M. Nazem, and M. Karakus, "Numerical analysis of a large landslide induced by coal mining subsidence," *Engineering Geology*, vol. 217, pp. 141–152, 2017.

[5] C. Yu, C. Han, R. Xie, and L. Wang, "Mechanical behavior analysis of buried pipeline under stratum settlement caused by underground mining," *International Journal of Pressure Vessels and Piping*, vol. 188, article 104212, 2020.

[6] Z. Jianjun, W. Xun, S. Yanbing, W. Jiangbo, and M. L. Lee, "Deformation behavior of mining beneath flat and sloping terrains in mountainous areas," *Geofluids*, vol. 2021, Article ID 6689966, 16 pages, 2021.

[7] J. L. Yu, J. J. Zhao, H. Y. Yan et al., "Deformation and failure of a high-steep slope induced by multi-layer coal mining," *Journal of Mountain Science*, vol. 17, no. 12, pp. 2942–2960, 2020.

[8] J. G. Zhang, W. Yang, B. Lin, J. J. Zhang, and M. Wang, "Strata movement and stress evolution when mining two overlapping panels affected by hard stratum," *International Journal of Mining Science and Technology*, vol. 29, no. 5, pp. 691–699, 2019.

[9] Q. Sun, F. Ma, J. Guo et al., "Excavation-induced deformation and damage evolution of deep tunnels based on a realistic stress path," *Computers and Geotechnics*, vol. 129, article 103843, 2021.

[10] Y. Wang, D. Liu, J. Han, C. Li, and H. Liu, "Effect of fatigue loading-confining stress unloading rate on marble mechanical behaviors: an insight into fracture evolution analyses," *Journal of Rock Mechanics and Geotechnical Engineering*, vol. 12, no. 6, pp. 1249–1262, 2020.

[11] Z. Zhang, M. Deng, J. Bai, X. Yu, Q. Wu, and L. Jiang, "Strain energy evolution and conversion under triaxial unloading confining pressure tests due to gob-side entry retained," *International Journal of Rock Mechanics and Mining Sciences*, vol. 126, article 104184, 2020.

[12] Z. Jiang, Q. Li, Q. Hu et al., "Acoustic emission characteristics in hydraulic fracturing of stratified rocks: a laboratory study," *Powder Technology*, vol. 371, pp. 267–276, 2020.

[13] B. Q. Li, B. Gonçalves da Silva, and H. Einstein, "Laboratory hydraulic fracturing of granite: acoustic emission observations and interpretation," *Engineering Fracture Mechanics*, vol. 209, pp. 200–220, 2019.

[14] P. Jin, E. Wang, X. Liu, N. Huang, and S. Wang, "Damage evolution law of coal-rock under uniaxial compression based on the electromagnetic radiation characteristics," *International Journal of Mining Science and Technology*, vol. 23, no. 2, pp. 213–219, 2013.

[15] A. Cao, G. Jing, Y. L. Ding, and S. Liu, "Mining-induced static and dynamic loading rate effect on rock damage and acoustic emission characteristic under uniaxial compression," *Safety Science*, vol. 116, pp. 86–96, 2019.

[16] Y. Liang, Q. Li, Y. Gu, and Q. Zou, "Mechanical and acoustic emission characteristics of rock: effect of loading and unloading confining pressure at the postpeak stage," *Journal of Natural Gas Science and Engineering*, vol. 44, pp. 54–64, 2017.

[17] C. E. Fairhurst and J. A. Hudson, "Draft ISRM suggested method for the complete stress-strain curve for intact rock in uniaxial compression," *International Journal of Rock Mechanics and Mining Sciences*, vol. 36, pp. 281–289, 1999.

[18] G. Gao, M. A. Meguid, and L. E. Chouinard, "On the role of pre-existing discontinuities on the micromechanical behavior of confined rock samples: a numerical study," *Acta Geotechnica*, vol. 15, no. 12, pp. 3483–3510, 2020.

[19] H. Kang, L. Wu, F. Gao, H. Lv, and J. Li, "Field study on the load transfer mechanics associated with longwall coal retreat mining," *International Journal of Rock Mechanics and Mining Sciences*, vol. 124, article 104141, 2019.

[20] A. Saeidi, S. Heidarzadeh, S. Lalancette, and A. Rouleau, "The effects of in situ stress uncertainties on the assessment of open stope stability: case study at the Niobec Mine, Quebec (Canada)," *Geomechanics for Energy and the Environment*, vol. 25, p. 100194, 2021.

[21] C. Zhang, X. T. Feng, and H. Zhou, "Estimation of in situ stress along deep tunnels buried in complex geological conditions," *International Journal of Rock Mechanics and Mining Sciences*, vol. 52, pp. 139–162, 2012.

[22] G. Feng and P. Wang, "Simulation of recovery of upper remnant coal pillar while mining the ultra- close lower panel using longwall top coal caving," *International Journal of Mining Science and Technology*, vol. 30, no. 1, pp. 55–61, 2020.

[23] M. Cai, P. K. Kaiser, Y. Tasaka, and M. Minami, "Determination of residual strength parameters of jointed rock masses using the GSI system," *International Journal of Rock Mechanics and Mining Sciences*, vol. 44, no. 2, pp. 247–265, 2007.